Available online at www.sciencedirect.com

ScienceDirect

Solid Earth Sciences 6 (2021) 27–36

www.elsevier.com/locate/SESCI

Morphological aspects, textural features and chemical composition of spherules from the Colônia impact crater, São Paulo, Brazil

Victor F. Velázquez [a,*], Celso B. Gomes [b], Marcos Mansueto [b], Leonardo A.S. de Moraes [b], José Maria A. Sobrinho [c], Rodrigo F. Lucena [a], Alethéa E.M. Sallun [c], William Sallun Filho [c]

[a] *Escola de Artes, Ciências e Humanidades, Universidade de São Paulo, Rua Arlindo Bettio, 1000, CEP 03828-000, São Paulo, Brazil*
[b] *Instituto de Geociências, Universidade de São Paulo, Rua do Lago, 562, CEP 05508-080, São Paulo, Brazil*
[c] *Instituto Geológico da Secretaria do Meio Ambiente, Rua Joaquim Távora, 822, CEP 04015-011, São Paulo, Brazil*

Received 20 July 2020; revised 18 November 2020; accepted 18 December 2020
Available online 4 March 2021

Abstract

A wide variety of spherules and aluminum-silicate accretionary particles are found associated to allochthonous breccia deposits within the Colônia impact crater, SE Brazil. Using morphological, textural and compositional variation parameters, four types of spherules can be identified: (i) iron spherules and (ii) silicate-iron spherules, both dominant, and scarce (iii) titanium-silicate-iron spherules and (iv) copper-nickel-iron spherules. The spherules range in size from 0.1 mm up to 0.5 mm, and exhibit noticeable splash kinematic shapes with variations for spherical, oval, prolate and droplet. Textural patterns include granular massive, polygonal junctions, and several types of dendritic growth. Iron spherules are mainly pure iron oxides (magnetite and/or hematite) and contain low contents in Mg, Na, K, P and also in REE; occasionally, they may contain Si and Mn. Silicate-iron spherules differ for the higher concentrations in Si and in a few times in Ti and Ca. The accretionary particles have nothing in common with the spherules, except for its close spatial and temporal occurrence. In terms of morphology, they do not show symmetric splash-form shapes and some of them are clearly composed of different parts of fine pieces of mineral fragments mechanically aggregated in a partially molten state before the deposition. Chemical composition of accretionary particles reveals abundance of the elements Si, Fe and Al, presence of K and less commonly of Ti, Ca, Na and P. Because these elements are found in great amounts in minerals of the regional country rocks, it is assumed that the formation of both splash-form spherules and accretionary particles is probably related to the melting of metamorphic lithologies of the crystalline basement due to hypervelocity impact event.

Keywords: Colônia crater; Impact spherules; Splash-form

1. Introduction

Spherules are discrete natural solid particles which can be less than a hundred micrometers to a few millimeters in diameter (Brown and Scriven, 1908). The first discovery of magnetic spherules deposits was in deep-sea sediments during the H.M.S. Challenger expedition (Murray and Renard, 1891). A few years later, various other similar deposits were found in different geological settings: desert sand (Fredriksson and Gowdy, 1963), beach sediments (Marvin and Einaudi, 1967) and even in the Antarctic ice sheet (Wagstaff and King, 1981). Those spherules were often described as being of extraterrestrial origin, micrometeorites or comet dust. With the improvement of analytical tools used to non-destructively determine the chemical composition of small volumes of solid materials was possible to recognize three main groups: a) metallic spherules, b) silicate spherules e c) glass spherules (Ma et al., 1987). After this initial precursor phase, several researchers have reported the occurrence of spherules or spherule layers as being of cosmic, volcanic, impact and

* Corresponding author.
E-mail address: vvf@usp.br (V.F. Velázquez).
Peer review under responsibility of Guangzhou Institute of Geochemistry.

https://doi.org/10.1016/j.sesci.2020.12.004

industrial origin (Guaita and Martegani, 2008; Niyogi et al., 2011; Glass and Simonson, 2012; Genareau et al., 2015). Impact spherules are nearly spherical droplets that can be formed in two ways: as metal-silicate splash particles of ejected impact melt and as condensates from the rock-vapor plume (Johnson and Melosh, 2012). Glassy spherules that do not contain any crystallites are called microtektites and commonly originated as melt spherules which cooled too quickly forming glass bodies (Glass, 1990; Glass and Simonson, 2013). In contrast, crystal-bearing spherules are typical to have originated from vapor condensates which cooled slowly enough to form spherules with microlites of primary minerals and are termed microkrystites (Glass and Burns, 1988; Ebel and Grosmman, 2005). According to Glass and Simonson (2013), the glass spherules originated from the impact-generated melts are generally heterogeneous and can incorporate unmelted or partially melted mineral grains. Individual layers rich in spherules interpreted as distal impact ejecta are well-known in the literature. The first records documented as such are the occurrence of Barberton greenstone belt, South Africa, and Warrawoona Group, Western Australia, both of Paleoarchean age (Glass and Simonson, 2012). In many cases, these deposits are the only records of the existence of an ancient impact and it is therefore of great importance to understand the conditions under which the spherules were generated and its relationship with the cratering process (Simonson and Glass, 2004; Johnson and Melosh, 2012).

In studies performed by Velázquez et al. (2018) were reported the occurrence of spherules in association with allochthonous breccia deposits within the Colônia impact crater. This paper presents a detailed study of the morphology, texture and chemical composition of these spherules helping to elucidate their origin.

2. The Colônia crater

Spherules and accretionary particles are found in allochthonous breccia deposits in the interior of the Colônia crater (23°52′03″S and 46°42′27″W), a circular morphological feature spreading over an area of 10.2 km^2 that lies in the region of Parelheiros, approximately 40 km SW from the center of São Paulo city, Brazil (Fig. 1A; Velázquez et al., 2018). It has been proposed by several authors (Kollert et al., 1961; Crósta, 1987; Riccomini et al., 1989, 1991, 1992, 2005, 2011; Masero and Fontes, 1992; Velázquez et al., 2010, 2013) that this depression was originated by the impact of a large extraterrestrial body, leading to the formation of a huge hole with 3.6 km rim-to-rim diameter in crystalline basement rocks of Neoproterozoic age of the Ribeira Fold Belt (Hasui et al., 1975), mainly consisting of mica schists, quartzites, gneisses and migmatites (Coutinho, 1980). Presently, the depression is filled with organic-rich silty clay of Quaternary age, minor intercalations of mudstone and Precambrian rock fragments, and it is partially covered by vegetation, remnants of an original forest. It forms a planned area with small hills up to 125 m higher than the inner swampy alluvial plain. The whole area has been in part occupied by a local community, the Vargem Grande district, clustering nowadays over 45,000 people. The crater, clearly evidenced by aerial photographs and satellite images (Fig. 1B and C), was primarily subject to a gravimetric/electrical resistivity survey by Kollert et al. (1961) that estimated the depth of the basement at the center of the depression between 285 and 400 m. Additional geophysical information (gravimetric, geoelectrical and seismic surveys) resulted from the papers by Masero and Fontes (1992), Motta and Flexor (1991) and Neves (1998). Based on new seismic data, Riccomini et al. (2011) suggested for the crater a sedimentary fill of approximately 275 m thickness. Over recent years, boreholes drilled inside the depression for groundwater exploration reached depths up to 197 m in crystalline rocks. Furthermore, the Basic Sanitary Company of São Paulo State (SABESP), aiming to supply drinking water for the local community, put in operation in March 2014 a conventional vertical drilling project 304 m long (drilling 3 in Fig. 1C) that, however, did not reach the basement.

Direct evidence for the impact origin of Colônia was provided and discussed for the first time by Velázquez et al. (2010, 2013). These authors described a series of distinctive shock-metamorphic features, including planar deformation on minerals, ballen quartz with heterogeneous extinction, granular extinction in zircon crystals and melt-bearing impact rocks. In addition, Velázquez and their collaborators have spent a great deal of work in the study of the crater, calling especially the attention for the needs of its preservation as a natural patrimony (Velázquez et al., 2006, 2008, 2014).

3. Sampling and analytical methods

Recovery material from the borehole 3, collected at each 2 m interval, consisted of a heterogeneous and discontinuous petrographic association basically having non- and fractured/brecciated crystalline rocks, lithic fragments and mineral clasts in addition to some intercalations of terrigeneous, organo-pelitic sediments. Spherules are found in the interval of 180–224 m depth, being, however, more frequent at the level of 198 m depth (Fig. 2). From the whole set of collected microspherules, 20 out of a total of 50 were selected for the characterization of morphological features and chemical composition analyses.

A simple elutriation technique was used to remove fine particles (<0.01 mm), being the sample size higher than 0.35 mm and lower than 1 mm. Samples were dried at 80-90 °C temperature and separation of spherules employed a binocular stereomicroscope of 100x magnification.

Chemical analyses were determined by a Jeol JXA-8530F field emission electron microprobe utilizing both EDS and WDS systems. Analytical conditions comprised acceleration voltage of 15 kV, beam current of 20 nA and beam diameter of 5 μm. For the X-ray secondary images electronic conditions were 10–15 kV and 200–400 pA, respectively. Images magnification ranged from 40 to 25,000 times. As analytical standards were employed synthetic material (REE phosphate

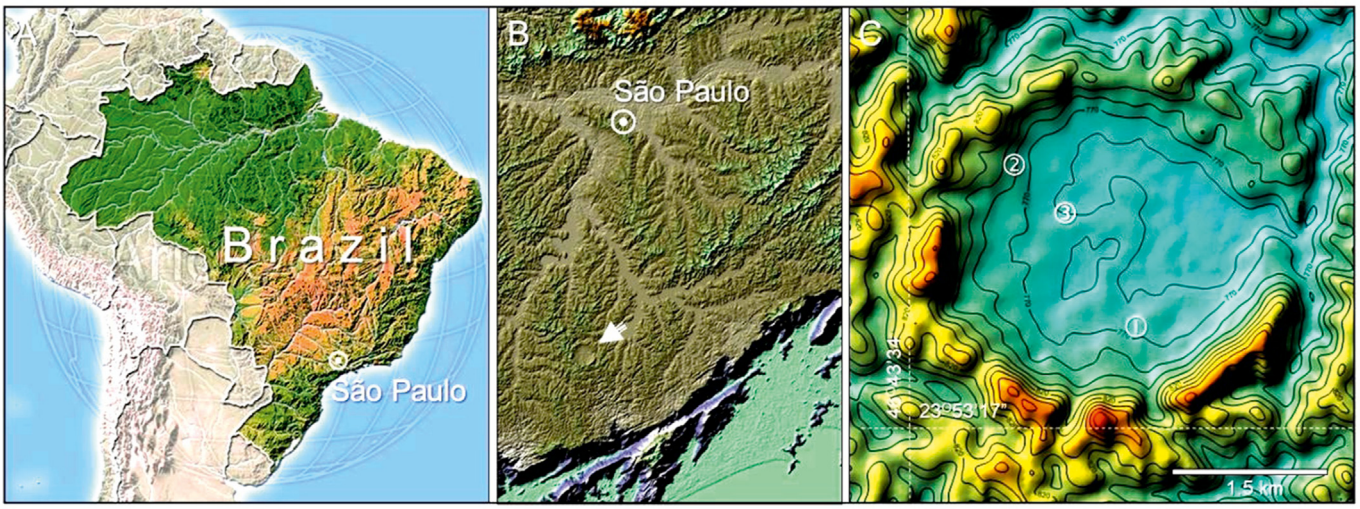

Fig. 1. Location of the study area (A and B) and morphological aspect of the Colônia impact crater (C). The numbers show the sites of the boreholes within the structure: 1, 270 m, Riccomini et al. (2011); 2, 197 m, Velázquez et al. (2013); 3, 304 m (Velázquez et al., 2018).

and rhyolitic glasses) and different minerals made available by the National Museum of Natural History, Smithsonian, Washington D.C. For information on the standards see paper by Jarosewich et al. (1980).

4. Morphological aspects

Individual spherules are characterized by a wide variety of sizes and shapes. The spherules range in size from 0.1 mm up to 0.5 mm, the most prevalent value being 0.5 mm. Adopting the geometrical analysis criteria previously proposed by Stauffer and Butler (2010) to study the shapes of splash-form tektites, the spherules can be characterized as a typical splash kinematic shape with variations for spherical, oval, droplet, and, less often, prolate (Fig. 3). Different shapes and surface marks are conspicuous features. Previous studies from the literature (Brown and Scriven, 1980; Elkins-Tanton et al., 2003; Butler et al., 2011) indicate that these features result of different spinning speed during the freezing of the droplets of molten rock ejected, leading to a continuous formation of aerodynamic rotational splash shapes. Agglutinated forms made up of two or more spherules melted together were also noticed (Fig. 3F, G and K). In this case, the spherules display a crushed contact surface (Fig. 3F), suggesting that the particles collided in a partially molten state under aerodynamic conditions.

The external surface of spherules may range from shiny, overshadow, smooth, rough and striated, and in most cases is covered by microcraters and pits. The former are small circular depressions that distort the flat surface of the spherules whereas the pits are tiny hollow with radial cracks showing a wide diversity of shapes (irregular, circular or rarely star). The microcraters and pits represent clear evidence of successive stages of post-solidification collision (Prasad and Sudhakar, 1998; Prasad and Khedekar, 2003). The stria marks consist of a set of fine parallel lines with contorted appearance exposed on the surface of spherules and are interpreted as schlieren structures generated from liquid droplet.

A large number of accretionary particles occur associated with the spherules. The particles have different shapes, sizes and colors, with the major axis slightly larger than 0.4 mm and the color mostly varying from yellowish brown to dark reddish brown. Unlike the spherules, the accretionary particles exhibit several bubbles on the surface, chaotic features of plastic flow and markedly curved edges (Fig. 4). Bubbles or vesicles are interpreted according to Belza et al. (2017) as outgassing of volatile components rapidly exsolving from the melt during quenching. The presence of relict grains without bubbles seems to indicate that they have not melted completely during the formation process. Some particles are clearly formed of different parts that presumably would have agglutinated in a partially molten state before the deposition.

5. Textural features

SEM images were employed to detail the topographic contrasts of the spherules and accretionary particles. The relation between size and shape of the grains as well as the microfabrics that result from the interlaced pattern arrangement are used to support some inferences about the texture of spherules. Based on these parameters, it is possible to distinguish three types of surface texture: smooth, moderate and rough. Spherules with smooth texture show compact crystalline structure, flat and polished surface (Fig. 5A) and are composed of fine grains interlaced of random arrangement with trapped frozen fluids in the interstices (Fig. 5B). The interstitial phase exhibits a variety of quench texture only developed by a liquid that has not reached the critical initial step of nucleation to trigger crystallization. Thus, this textural pattern represents an important evidence supporting the hypothesis that such a splash-shape spherule would have been formed by a quick cooling of rotational molten droplets. The

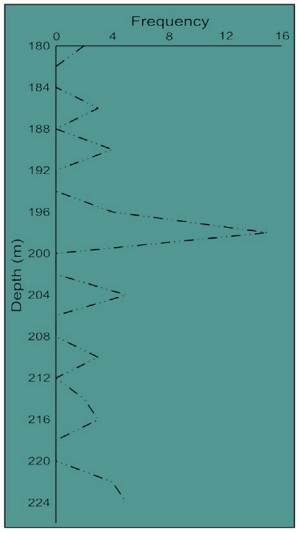

Fig. 2. Frequency polygon illustrating the relationship between the depth and the relative abundance of spherules from 50 samples.

other two textures display very different patterns: moderate with a surface slightly wavy (Fig. 5C) and rough with a surface uneven or irregular (Fig. 5F). A polygonal pattern was most commonly noted in spherules with moderate surface texture (Fig. 5C and D). This pattern is formed of magnetite grains that are all approximately of the same size, and the face-to-face junction follows the symmetry elements involved in the crystal face (Fig. 5E). Assuming that the volume of the droplets remains constant during the cooling and considering that the grains exhibit well-developed faces, with the grain size varying slightly, the texture is interpreted as evidence of a morphological change from an initial droplet shape to a "soccer ball-like shape" faceted under slow cooling crystallization conditions. Lastly, the spherules with rough surface texture are mostly composed of grains dendritic and skeletal plates with variable arrangement (Fig. 5G). A wide range of random dendritic patterns, in particular the lateral branches, has been observed and detailed images are found in some spherules of Fig. 6. Dendritic crystals radiating from a single point at the edge of the spherules are common; however, in some cases the branching reveals a clear dissemination from the border to the center of the spherules. A set of fine parallel striations can be associated to the dendritic arms (Fig. 5H). Dendritic structures of minerals are related to growth conditions, especially cooling rates, being their formation due to the very rapid cooling of molten material (Flemings, 1974; Xu, 2004; Glicksman, 2011).

The external textures of the accretionary particles usually differ from those of splash-shape spherules (Fig. 7). In general, the polished sections reveal a heterogeneous morphology on all scales. The angular particles are accreted grain clusters in a fine matrix of fluidal texture masked by red-brown iron oxide originated from rocks intensely crushed. Therefore, the fragments may include small pieces of preexisting rocks, mineral fragments, and other debris. Although the features of the textural framework may seem insufficient, petrographic evidence documented by Velázquez et al. (2018) support that the accretionary particles had an impact origin.

6. Chemical composition

The concentration of major and minor oxides and some trace elements of all investigated spherules and accretionary particles is listed in Table 1 and the spot analysis position shown in Figs. 6 and 7. In terms of compositional variation, four types of spherules with striking differences in content of major elements can be distinguished: (i) iron spherules (MS-Gr-1, 4, 12), (ii) silicate-iron spherules (MS-Gr-3, 8, 10, 16), (iii) titanium-silicate-iron spherules (MS-Gr-15), and (iv) copper-nickel-iron spherules (MS-Gr-13). Iron spherules have usually iron oxide content (Fe expressed as Fe_2O_3) higher than 97 wt% and very low concentration for the other elements. They are considered to be pure iron oxide minerals, such as magnetite and hematite. Regarding silicate-iron spherules, the main chemical changes are related to the Si concentration, ranging between 0.5 and 26 wt%. Fe is present in the iron oxide crystals and Si occurs in different proportions in the matrix. Some iron oxide crystals show Ca content up to 4 wt%. Substantial compositional differences were registered for the titanium-silicate-iron spherules, exhibiting expressive enrichment in Si, Ti, Ca and at lesser extent in Al and Mn. The main variations are usually the high Ti content (>4 wt%) and the significant presence of Si (5.4–24 wt%), Al (0.9–5.2 wt%) and Mn (2.1–3,9 wt%). Samples of this group (MS-Gr-2 and MS-Gr-15) contain high Fe (>60%), Ca (>19 wt% and >6.6 wt%, respectively) and Zr (MS-Gr-15, >9.8 wt%) concentrations, whereas Mg, Na, K and P are present in low amounts or below the detection limit. The copper-nickel-iron spherules are represented by an unique sample showing the highest abundance in Ni (28–31 wt%) and Cu (11–15 wt%). These elements are believed to be incorporated into the iron oxide crystals and within the matrix. The Fe content in the sample is less than 60 wt% and, similar to the other spherules, Mg, Na, K and P are only present in small amounts (Table 1).

The accretionary particles are characterized by a much more heterogeneous composition when compared to the spherules. In general, they exhibit high contents in Si, Al, Fe and K (Table 1) and based on the concentration of these elements, three types of dominant chemical composition can be distinguished: (i) aluminum-silicate accretionary particles (AP-Gr-1), (ii) aluminum-iron-silicate accretionary particles (AP-Gr-3, 8, 10) and (iii) aluminum-potassium-silicate accretionary particles (AP-Gr-5). The data available for the first type indicate at least three distinct components, two crystalline phases with marked compositional difference and one phase that mostly occurs in the submicroscopic matrix (Fig. 7A). Judging from the high contents of Si and Si–Al, the crystalline minerals are thought to be discrete fragments of quartz and of an aluminum-rich phase set in a fine matrix made up by Si, Al, Fe and Ca. Aluminum-iron-silicate-rich accretionary particles include samples greatly variable in composition. For the different crystalline phases, the variation is mainly related to the Si, Al, and K concentrations. Thus,

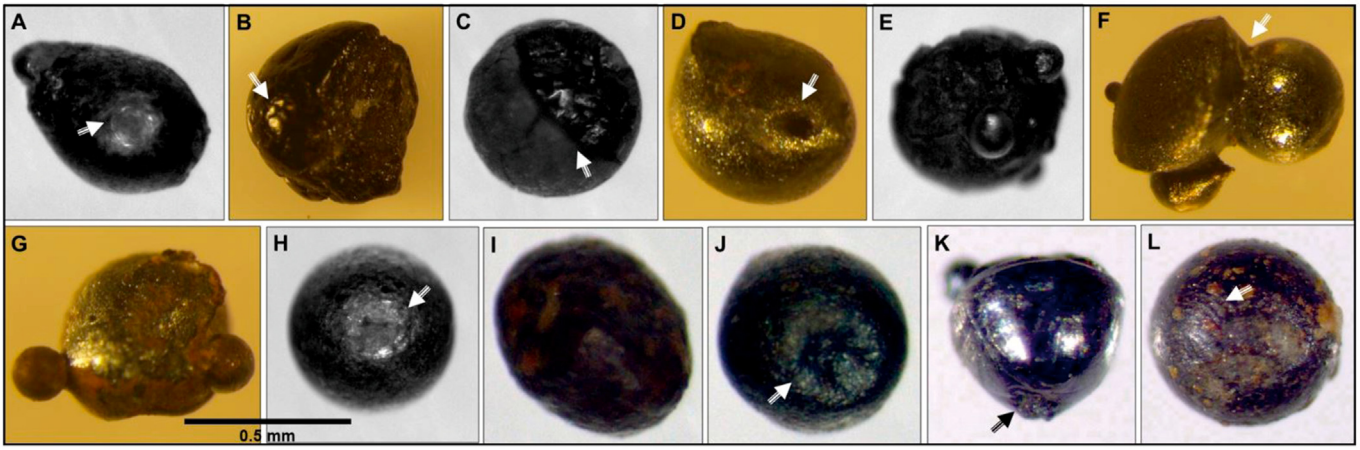

Fig. 3. Stereomicroscope images of several splash kinematic shapes common to the spherules, including spherical (H, J and L), oval (I), prolate (A) and droplet (D). Agglutinated forms are shown in E, F, G and K. In F, the arrow points to the junction surface between spherules. Presence of microcraters is observed in A, H, J and L. Primary star-shaped pit can be noted in B and other pits with more irregular appearance in D and K.

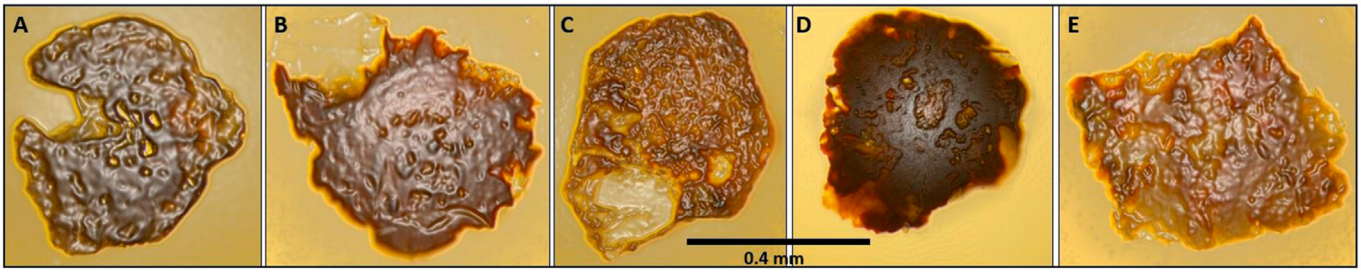

Fig. 4. Accretionary particles with various marks and features on the surface. All display chaotic surface, curved edge and plastic fluidal texture. Shaded relief based on stereomicroscope digital images: original color and natural brightness, vertical lighting source, roughness contrast 3%.

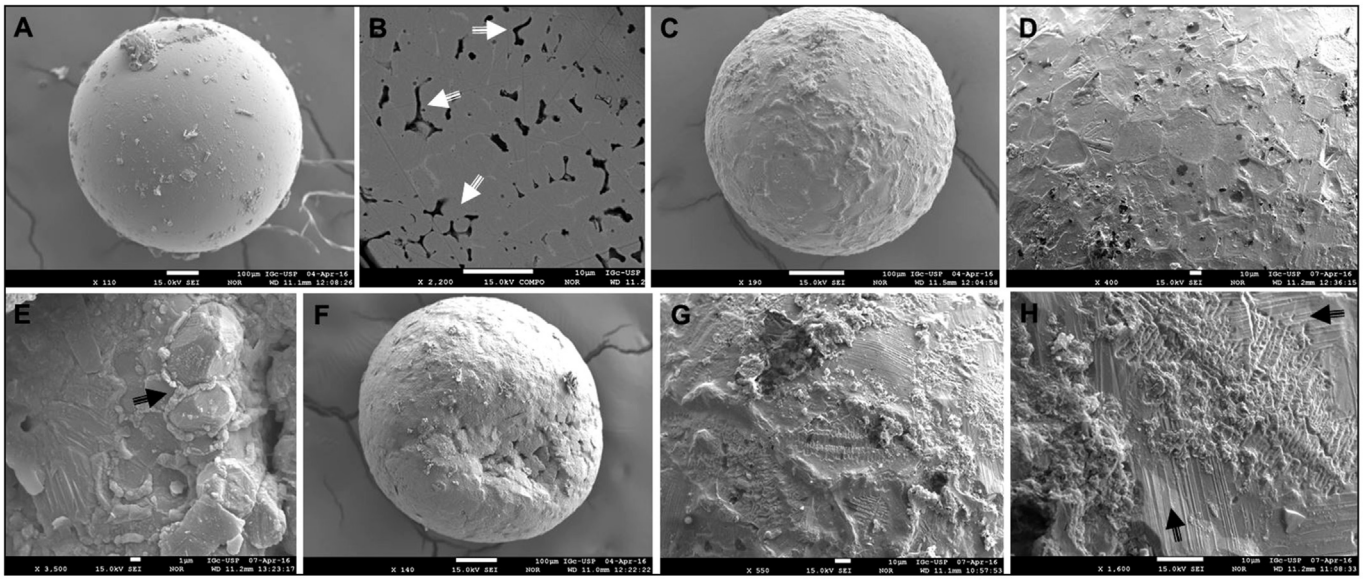

Fig. 5. SEM images of spherules illustrating the morphological aspects and some surface features. A) Perfect spherical shape and smooth surface. B) Detail of smooth surface in A showing a compact mosaic of fine crystals with trapped frozen fluids in the interstices (white arrow). C) Spherical shape and moderate surface with polygonal pattern. D and E are enlarged images of "soccer ball-like shape" with clear evidence of a face-to-face junction of the magnetite crystals (black arrow). F) Slightly oval shape and rough surface, mostly composed of grains dendritic and skeletal plates, which are more evident in G. H) Set of fine parallel striations is noticeable among the dendritic arms (black arrows).

high Al–K content suggests the occurrence of remaining crystals of alkali feldspar and Si concentrations more than 97 wt% indicate the presence of small relict grains of quartz. Except for the AP-Gr-10-7 sample, which has a Ti content greater than 75 wt%, the matrix of these materials is essentially formed, in order of abundance, by Fe, Si, Al and P. Aluminum-potassium-silicate-rich accretionary particles contain basically the same crystalline phases, being in general enriched in Al–K. Although the matrix components are not proportionally identical, there is good similarity with respect to the main chemical characteristics, including the variable contents of Fe, Si, Al and P. In the whole set of samples, spherules and accretionary particles reveal essentially an abundance of three oxides: silica, iron oxide and aluminum oxide. The representation of these components in a Fe_2O_3–Al_2O_3–SiO_2 ternary diagram (Fig. 8A) shows a clear concentration of samples along the Fe_2O_3–SiO_2 and Al_2O_3–SiO_2 sides. Similar behavior was registered for the Fe_2O_3–CaO + MgO + TiO_2–SiO_2 and Al_2O_3–CaO + MgO + TiO_2–SiO_2 diagrams (Fig. 8B and C, respectively). Although variations for these elements do exist between the two groups, the chemical affinity seems to be evident. Therefore, the similar behavior noticed for the major elements is a strong suggestion that both the spherules and accretionary particles would have a common origin.

7. Discussion and final considerations

During the hypervelocity impact craters formation, the kinetic energy of the bolide is transformed at the impact site into high-pressure shock waves and the impactor and target rocks are pulverized and ejected into a fireball cloud containing a mixture of vapor, melt products, shocked and unshocked rocks debris, and breccias (Grieve and Therriault, 2012; Osinski and Pierazzo, 2012). Most of the material is expelled and deposited around the crater to form an ejecta blanket, but a part is straight up and falls back inside the crater, forming the so-called fallback ejecta (Melosh, 1989; Stöffler and Grieve, 2007). The deposits of impact ejecta, distal or fallback, generally form thin layers and they can contain sand-sized spherical particles or smaller known as impact spherules (Simonson and Glass, 2004). According to Johnson and Melosh (2014), impact spherules are formed from vaporized material or impact melt products, within high temperature impact plumes, which afterward would have cooled quickly in aerodynamic conditions. Impact spherules occur in a wide variety of forms, including spheres, ellipsoids, oblates, flat discs and dumbbells, and some authors have proposed that such forms resulted from the combined action of surface tension and centrifugal forces that acted during the rotation of the fluid droplets (Brown and Scriven, 1980; Elkins-Tanton et al., 2003; Stauffer and Butler, 2010; Butler et al., 2011).

Discrete layers containing impact melt-bearing impactites were described by Velázquez et al. (2018) from allochthonous breccia deposits within the Colônia impact crater. Impact melt products comprise different petrographic types generated under high pressure and temperature conditions from the regional country rocks of the crystalline basement. A wide variety of iron spherules and aluminum-silicate accretionary particles occur associated in a similar way to those spherules previously described in the literature from other localities. Based on a careful examination of their shape, microstructure,

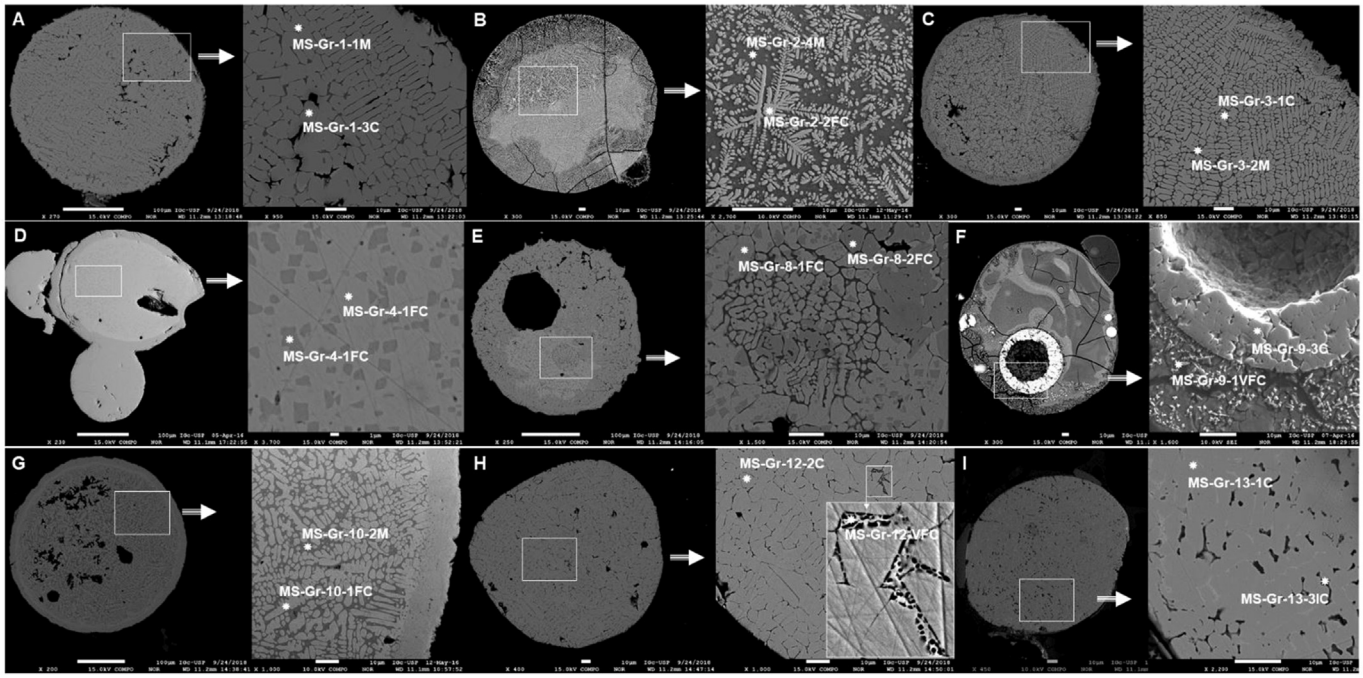

Fig. 6. SEM images of polished sections of several spherules showing a wide variety of textural arrangement and dendritic growth. Alphanumeric identification is as in Table 1 and the asterisk indicates the beam position.

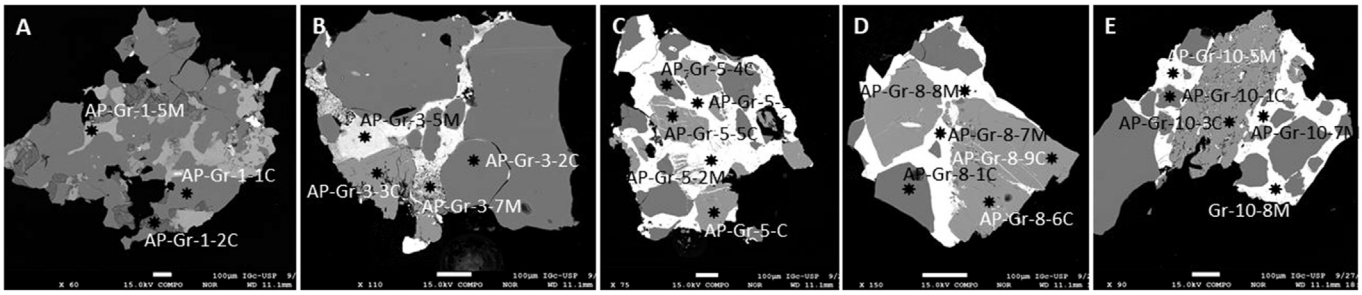

Fig. 7. SEM images of polished sections of some accretionary particles illustrating a large number of different crystalline phases immersed in a fine heterogeneous matrix. Alphanumeric identification is as in Table 1 and the asterisk indicates the beam position.

texture and chemical composition, four main groups can be recognized: (i) iron spherules, (ii) silicate-iron spherules, (iii) titanium-silicate-iron spherules, and (iv) copper-nickel-iron spherules. The most distinctive characteristics of the spherules are: 1) morphology, which can be found in different "splash-forms" ranging from perfect spheres to oval, droplet and prolate. Fused or agglutinated spherules may also be present. Numerical model performed by Stauffer and Butler (2010) and research conducted on fluid dynamical in laboratory by Elkins-Tanton et al. (2003) have shown that such forms result from the way in which molten drops spun in free rotation conditions; 2) microstructure and surface sculpturing, these are peculiar destructive marks (microcraters and pits) that stand out on the surface of the spherules, usually interpreted as due to successive collisions in free flight after solidification (Prasad and Sudhakar, 1998; Prasad and Khedekar, 2003). Accounting on the size of the spherules (˜0.5 mm) and, in particular, the shape and depth of impact marks, it is assumed that the particles would have collided at very high speed; and 3) texture and microfabric, these are characterized by the variation of size, shape and preferential distribution of the mineral grains, being possible to distinguish at least three different textural types: (i) allotriomorphic granular or granular massive, consisting of randomly oriented interlocking grains with some interstitial frozen fluids; (ii) polygonal junctions, crystals with well-developed faces tending to form triple junctions at 120-degree angles; and (iii) dendritic patterns, they develop whenever the formation of crystals with regular faces is replaced by the growing and agglutination of tiny grains forming several branches. In a broader context, these textural patterns are highly suggestive of a significant fluctuation of the thermodynamic conditions (P-T) that would have directly influenced in the cooling rate and in the dynamic of crystallization of the minerals during the solidification of iron spherules, as proposed by Belza et al. (2017) for the distal spherules from the K-T boundary in the Umbria-Marche region, Italy.

In terms of morphology appearance, the accretionary particles have nothing in common with the iron spherules, except for its special and temporal occurrence. They do not exhibit symmetric splash-form shapes and are clearly composed of different mineral fragments that presumably would have mechanically aggregated in a partially molten state before the deposition. These particles have microgranular accretionary fabric and the most frequent mineralogical assemblage contains quartz and feldspar grains set in an aluminum-iron silicate matrix. Plastic flow of chaotic aspects and a large number of bubbles are recognized. Most of the described textural features present similarities with the descriptions given by Addison et al. (2005) for the melt fragments and impact accretionary material forming the Sudbury ejecta, Canada.

The chemical compositions suggest that both iron spherules and accretionary particles have substantial major-element compositional heterogeneity. One of the most striking observation is that spherule samples contain usually great amount of Fe and low concentration of Mg, Na, K and P, suggesting a possible volatilization of these elements during the initial high temperature phase. Also, they are typically REE-poor. Some other spherules are characterized by expressive enrichments in Si, Ti, Ca and at lesser extent in Al and Mn. Only one sample is considerably abundant in Ni and Cu. Substantial variations in Fe–Si and Al–Si contents are registered in all accretionary particles. However, some of these samples can also show a significant enrichment in Ca and K. This compositional difference is in a greater or lesser degree due to the presence of relict mineral grains, mainly quartz and feldspar, in the mineralogical assemblage. Because these elements are very common in silicate minerals (quartz, feldspar and mica) it is quite reasonable to assume that both splash-form spherules and accretionary particles would have formed from the melting of crystalline basement rocks.

As pointed out early, the spherules can be originated by different ways in nature: cosmic, volcanic, anthropogenic and impact-related melting of terrestrial target rocks. Arguments favoring the latter hypothesis are as follow: 1) dominant rotational splash-forms of the spherules (Fig. 9) are considered by several authors (Elkins-Tanton et al., 2003; Prasad and Khedekar, 2003; Stauffer and Butler, 2010) as primary evidence to distinguish impact spherules of other naturally occurring, except those of volcanic origin (Glass and Simonson, 2013); 2) surface sculpturing or impact marks (microcraters, pits with radial cracks and star-shaped pit) have been used as an important criterion to identify spherules of impact origin (Glass, 1974; Prasad and Sudhakar, 1998); 3) dendritic patterns and interstitial frozen fluids in granular massive texture, similar to those described by Blau et al.

Table 1
Representative analyses of major and minor oxides and some trace elements of spherules and accretionary particles. Alphanumerical identifications indicate the nature of sample (MS, microspherules; AP, accretionary particles), the beam position (Gr-1-1) and the analyzed material (C, crystal; CC, coarse crystal; FC, fine crystal; VFC, very fine crystal; M, matrix).

Sample/Position	Material	SiO_2	TiO_2	Al_2O_3	Fe_2O_3	MnO	MgO	CaO	Na_2O	K_2O	P_2O_5	V_2O_3	Cr_2O_3	NiO	CuO	ZnO	SrO	Y^2O_3	ZrO_2	Nb_2O_3	Cs_2O	Ce_2O_3	La_2O_3	HfO_2	Total
MS-Gr-1-3C	Iron spherule	1.99	0.08	0.20	100.65	0.75		0.10	0.14	0.02		0.00	0.01		0.03		0.04		0.04						104.05
MS-Gr-1-1M		0.28	0.06	0.17	103.10	0.59	0.01	0.02	0.01		0.06		0.02			0.01						0.02		0.02	104.37
MS-Gr-2-2FC	Titanium-	11.77	4.57	0.96	64.16	2.08		19.84		0.01	0.13	0.02	0.06		0.01	0.01	0.08						0.03	0.06	103.78
MS-Gr-2-4M	silicate-iron spherule	12.62	4.37	1.46	64.79	2.40		19.59	0.01	0.01		0.04	0.03	0.01	0.05		0.05		0.02	0.08		0.02	0.05		105.60
MS-Gr-3-1C	Silicate-iron	3.42	0.14	0.14	103.14	0.24	0.00		0.08		0.15	0.00	0.13	0.02			0.01					0.03			107.50
MS-Gr-3-2M	sphereule	26.29	0.11	0.33	81.65	0.70		0.02		0.01	0.20		0.01	0.02	0.02	0.00	0.01		0.01	0.01		0.00		0.01	109.41
MS-Gr-4-1FC	Iron spherule	0.22		0.03	106.72	0.94					0.26	0.01	0.03	0.02	0.08	0.03	0.03		0.01	0.01					108.39
MS-Gr-4-1FC		0.26		0.07	104.50	0.37		0.01	0.01		0.00	0.02	0.01	0.00		0.04					0.00	0.04			105.34
MS-Gr-8-1FC	Silicate-iron	0.53		0.17	101.62	0.25	0.01	0.02	0.02	0.01			0.91	0.02	0.01								0.04		103.62
MS-Gr-8-2FC	spherule	8.65		0.40	95.04	0.36	0.02	0.05	0.01	0.02	0.14		0.05	0.02	0.02		0.03		0.03	0.01	0.01	0.02	0.02	0.01	104.91
MS-Gr-9-1VFC	Silicate-titanium-	19.39	21.63	1.73	21.94	9.84	2.02	4.42	0.12	0.13	0.42	0.42	0.09	0.09	0.48	0.01			0.02	0.33		0.05	0.02	0.07	83.22
MS-Gr-9-3C	iron spherule	0.11	1.03	0.14	99.21	0.37	0.18	0.34	0.00	0.00	0.21	0.21	0.13	0.50	0.04	0.04	0.04		0.01	0.02			0.03		102.60
MS-Gr-10-1FC	Silicate-iron spherule	2.71	0.02	0.03	105.81	0.59	0.03	0.00		0.00	0.06		0.16	0.03	0.02			0.03	0.01	0.04					109.54
MS-Gr-10-2M		26.16		0.28	78.81	1.56		0.00	0.15	0.12	0.30		0.03	0.01	0.07		0.05		0.05	0.02		0.01		0.02	107.64
MS-Gr-12-2C	Iron spherule	1.55	0.05		101.48	0.57	0.03		0.03		0.08	0.00		0.02	0.05		0.00		0.05			0.03	0.02	0.03	104.00
MS-Gr-12-1VFC		0.24	0.16	0.01	102.39	0.55	0.02	0.01		0.00	0.04	0.03	0.07				0.05			0.00				0.04	103.61
MS-Gr-13-3C	Copper-nickel-iron	0.05			58.34		0.01				0.04	0.00	0.01	31.44	15.61			0.03		0.03		0.01			105.57
MS-Gr-13-1C	spherule	0.07	0.11	0.35	59.72			0.00	0.04		0.02		0.01	28.64	11.49	0.03	0.03		0.01	0.01			0.01		100.54
MS-Gr-15-1FC	Titanium-silicate-iron	5.41	14.14	1.99	76.12	2.29	0.01	1.59			0.08	0.13	0.11		0.05		0.02		3.04	0.05				0.09	105.12
MS-Gr-15-2M	spherule	24.07	17.13	5.22	32.93	3.90	0.00	6.69	0.00	0.01	0.45	0.19	0.01	0.00	0.02	0.02	0.04	0.00	9.85	0.23	0.04		0.00	0.11	100.91
MS-Gr-16-1C	Silicate-iron spherule	2.97	1.05	0.14	92.43	0.60	0.08	3.42	0.01	0.01	0.13	0.02	0.04	0.02	0.08		0.02	0.00							101.01
MS-Gr-16-2C		4.96	1.18	0.24	89.74	0.56	0.10	4.47		0.02	0.04	0.04	0.04		0.09	0.00	0.00		0.06			0.01	0.01	0.04	101.59
AP-Gr-1-1C	Aluminum-silicate	100.10		0.02	0.01	0.01			0.01		0.10	0.01	0.01	0.04			0.03					0.00			100.35
AP-Gr-1-5M	aggregate	38.55		29.61	5.90	0.20		23.76		0.02	0.07			0.02		0.01	0.31						0.03		98.45
AP-Gr-1-2C		46.11		51.67		0.32	0.01	0.12	0.31	0.07	0.14	0.05		0.01	0.05	0.11	0.05	0.04							99.06
AP-Gr-3-2C	Aluminum-iron-	100.31		0.01	0.02	0.01	0.01	0.00	0.03			0.00			0.01	0.02	0.06								100.48
AP-Gr-3-3C	silicate aggregate	64.39		18.42	0.18	0.02			0.58	15.92	0.60			0.02		0.01	0.03				0.08			0.01	100.26
AP-Gr-3-5M		5.48	0.09	3.26	66.13	0.16	0.29	0.55	0.05	0.04	2.67	0.06	0.00	0.00	0.01	0.11		0.00				0.00	0.01		78.92
AP-Gr-3-7M		3.85	0.03	2.84	70.11	0.21	0.31	0.46		0.03	2.00	0.06	0.00	0.03		0.03	0.00			0.01		0.02			80.00
AP-Gr-5-1M	Aluminum-potassium-	7.76		2.13	71.64		0.36	0.34	0.02	0.05	3.37	0.00	0.04	0.00		0.05	0.02							0.04	85.82
AP-Gr-5-2M	silicate aggregate	8.15	0.08	2.27	72.52		0.56	0.31	0.08	0.26	2.95		0.02	0.01	0.01		0.06	0.04			0.01	0.02	0.00		87.33
AP-Gr-5-4C		101.19	0.03	0.03	0.58		0.01	0.01		0.00	0.14		0.04				0.03		0.05			0.02		0.03	102.15
AP-Gr-5-5C		64.37	0.13	18.34	0.41		0.01		0.66	15.88	0.05	0.02	0.03		0.02	0.03	0.00			0.02			0.03		100.01
AP-Gr-5-6C		64.40	0.08	18.29	0.21			0.02	0.74	15.69	0.12					0.02	0.04		0.00						99.60
AP-Gr-8-1C	Aluminum-iron-silicate	64.24		18.29	0.59				0.73	15.72					0.04	0.01	0.02					0.01			99.65
AP-Gr-8-6C	aggregate	8.32	0.19	1.14	70.98	0.01	0.22	0.44	0.01	0.06	2.60	0.01	0.01	0.02						0.02		0.01	0.03	0.05	84.11
AP-Gr-8-7M		8.20	0.02	1.09	71.95	0.02	0.25	0.40	0.24	0.07	2.16		0.01	0.00	0.02			0.00							84.45
AP-Gr-8-8M		6.68		1.37	76.69		0.24	0.65	0.07	0.09	3.83	0.04	0.00	0.01				0.01				0.02	0.07	0.00	89.78
AP-Gr-8-9C		69.17		28.33	0.07	0.02			0.62	10.03	0.01	0.02		0.00	0.04		0.10			0.03				0.00	108.42
AP-Gr-10-1C	Aluminum-iron-silicate	100.51	0.08	0.01	0.76		0.00		0.01	0.00	0.06								0.04	0.01	0.03			0.05	101.57
AP-Gr-10-3C	aggregate	64.05		18.77	0.14	0.01		0.01	0.64	15.99	0.76	0.00	0.00				0.01			0.02	0.03			0.05	100.50
AP-Gr-10-5M		6.92		2.21	73.51	0.06	0.27	0.29	0.03	0.16	1.32	0.03	0.01			0.03				0.03					84.87
AP-Gr-10-7M		1.51	77.24	1.02	11.80	0.04	0.10	0.69	0.11	0.05	1.33	0.51	0.36		0.03	0.01				0.25					95.04
AP-Gr-10-8M		6.40		1.60	74.52	0.02	0.31	0.25	0.01	0.01	1.53	0.02	0.01			0.04		0.00				0.04		0.03	84.78

Alphanumerical identifications indicate the nature of sample (MS, microspherules; AP, accretionary particles), the beam position (Gr-1-1) and the analyzed material (C, crystal; CC, coarse crystal; FC, fine crystal; VFC, very fine crystal; M, matrix).

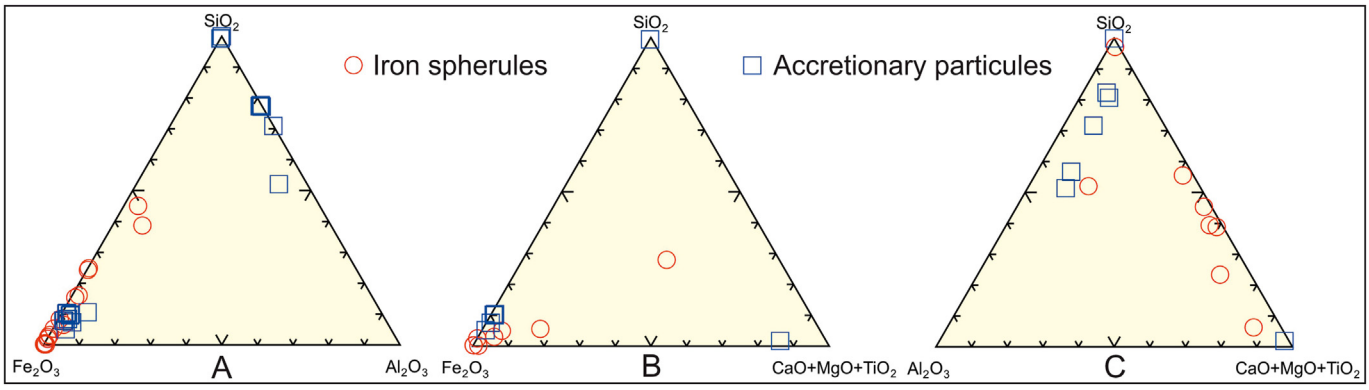

Fig. 8. Ternary diagram comparing the chemical composition between the spherules and accretionary particles. A) Fe_2O_3–Al_2O_3–SiO_2 system, B) Fe_2O_3–CaO + MgO + TiO_2–SiO_2 system and C) Al_2O_3–CaO + MgO + TiO_2–SiO_2 system. With some exceptions, there is a general trend of compositional affinity that follows an overlay line between the composition of the different groups.

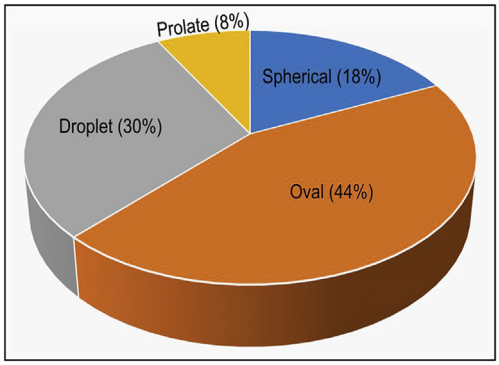

Fig. 9. Pie chart showing the relative abundance for some kinds of plash kinematic shapes from 50 spherules.

(1973) and Wu et al. (2013), are highly indicative that iron spherules were produced by high-temperature melting and quickly frozen afterwards; 4) the vast majority of samples (except MS-Gr-13) have low concentration in Cr–Ni and REE, eliminating a cosmogenic origin for the spherules; 5) similarly, the low concentration of Si, Al, Na, and K is markedly different from those of volcanic origin (obsidian, rhyolite), usually peraluminous and SiO_2-oversatured in composition (Heide et al., 2001; Cicconi and Neuville, 2019); 6) the Mn–Zn concentrations are significantly lower than expected for spherules of industrial origin (cf. Zhang et al., 2014); 7) similar behavior of the major elements (with preference for Fe_2O_3–Al_2O_3–SiO_2) in both iron spherules and accretionary particles supports the hypothesis of a common ballistic origin; 8) most convincing record consists in the limited occurrence of spherules in the lower layers of the sediment deposits filling the crater.

Declaration of competing interest

The authors declare that they have no known competing financial interest or personal relationships that could have appeared to influence the work reported in this paper.

Acknowledgments

We received help from a large number of people during the preparation of this paper. We are grateful to the colleagues of both institutions, EACH-USP and IG-SMA, for their help and support. W. Sallun Filho thanks the CNPq agency for a research grant. We also grant to the anonymous referees who substantially improved the quality of the manuscript. This study has been supported by the Fapesp agency (Procs. 2011/50987–0 and 2012/50042–9).

References

Addison, W.D., Brumpton, G.R., Vallini, D.A., McNaughton, N.J., Davis, D.W., Kissin, S.A., Fralick, W.P., Hammond, L.A., 2005. Discovery of distal ejecta from the 1850 Ma Sudbury impact event. Geology 33 (3), 193–196. https://doi.org/10.1130/G21048.1.

Blau, P.J., Axon, H.J., Goldstein, J.I., 1973. Investigation of the Canyon Diablo metallic spheroids and their relationship to the breakup of the Canyon Diablo meteorite. J. Geophys. Res. 78, 363–374.

Belza, J., Goderis, S., Montanari, A., Vanhaecke, F., Claeys, P., 2017. Petrography and geochemistry of distal spherules from the K–Pg boundary in the Umbria–Marche region (Italy) and their origin as fractional condensates and melts in the Chicxulub impact plume. Geochim. Cosmochim. Acta 202, 231–263.

Brown, R.A., Scriven, L.E., 1908. The shapeans stability of rotating liquid drops. Proc. R. Soc. A371, 331–357.

Butler, S., Stauffer, M., Sinha, G., Lilly, A., Spiteri, R., 2011. The shape distribution of splash-form tektites predicted by numerical simulations of rotating fluid drops. J. Fluid Mech. 667, 358–368. https://doi.org/10.1017/S0022112010005641.

Coutinho, J.M.V., 1980. Mapa geológico da Grande São Paulo, 1:100.000. São Paulo, Emplasa.

Cicconi, M.R., Neuville, D.R., 2019. Natural glass. In: Musgraves, J.D., Hu, J., Calvez, L. (Eds.), Springer Handbook of Glass. Springer Handbooks. Springer, Cham. https://doi.org/10.1007/978-3-319-93728-1_22.

Crósta, A.P., 1987. Impact structures in Brazil. In: Pohl, J. (Ed.), Research in Terrestrial Impact Structures. Friedrich Vieweg & Son, Braunschweig/Wiesbaden.

Ebel, D.S., Grosmman, L., 2005. Spinel-bearing spherules condensed from the Chicxulub impact-vapor plume. Geology 33 (4), 293–296.

Elkins-Tanton, L.T., Aussillous, P., Bico, J., Quéré, D., Bush, J.W.M., 2003. A laboratory model of splash-form tektites. Meteorit. Planet. Sci. 38, 1331–1340.

Flemings, M.C., 1974. Solidification processing. Metall. Trans. 5 (10), 2121–2134.
Fredriksson, K., Gowdy, R., 1963. Meteoritic debris from the Southern California desert. Geochim. Cosmochim. Acta 27, 241–243.
Genareau, K.J., Wardman, J., Wilson, T., McNutt, S., Izbekov, P., 2015. Lightning-induced volcanic spherules. Geology 43 (4), 319–322.
Glass, B.P., 1974. Microtektite surface sculpturing. Geol. Soc. Am. Bull. 85, 1305–1314.
Glass, B.P., 1990. Chronostratigraphy of upper eocene microspherules. Comment and reply. Palaios 5, 387–390.
Glass, B.P., Burns, C.A., 1988. Microkrystites: a new term for impact-produced glassy spherules containing primary crystallites. In: Ryder, G. (Ed.), Proceedings of the 18th Lunar and Planetary Science Conference. Cambridge University Press, Cambridge, pp. 455–458.
Glass, B.P., Simonson, B.M., 2012. Distal impact eject layers: spherules and more. Elements 8, 43–48.
Glass, B.P., Simonson, B.M., 2013. Distal impact ejecta layers. In: A Record of Large Impacts in Sedimentary Deposits. Springer-Verlag, Berlin-Heidelberg.
Glicksman, M.E., 2011. Principles of Solidification. Springer, New York.
Grieve, R.A.F., Therriault, A.M., 2012. Impactites: Their Characteristics and Spatial Distribution. John Wiley & Sons, Ltd., UK https://doi.org/10.1002/9781118447307.ch7.
Guaita, C., Martegani, F., 2008. Cosmic microsphere: a SEM study. Memorie della Supplementi 12, 110–125.
Hasui, Y., Carneiro, C.D.R., Coimbra, A.M., 1975. The Ribeira folded belt. Rev. Bras. Geoc. 5, 257–266.
Heide, K., Heide, G., Kloess, G., 2001. Glass chemistry of tektites. Planet. and Space Sci.v. 49, 839–844.
Jarosewich, E., Nelen, J.A., Norberg, J.A., 1980. Reference samples for electron microprobe analysis. Geostand. Newslet. 4, 43–47.
Johnson, B.C., Melosh, H.J., 2012. Formation of spherules in impact produced vapor plumes. Icarus 217, 416–430.
Johnson, B.C., Melosh, H.J., 2014. Formation of melt droplets, melt fragments, and accretionary impact lapilli during a hypervelocity impact. Icarus 228, 347–363.
Kollert, R., Björnberg, A., Davino, A., 1961. Estudos preliminares de uma depressão circular na região de Colônia, Santo Amaro, São Paulo. Bol. Soc. Bras. Geol. 3, 57–77.
Ma, S.L., Chai, C.F., Mao, X.Y., Peng, H.C., Lu, K., Xiao, X.Y., Ouyang, Z.Y., 1987. Identification of the origin of silicate, magnetic and glass spherules from the trace elemental abundances by INAA. J. Radioanal. Nucl. Chem. 114 (2), 329–335.
Masero, W.C.B., Fontes, S.L., 1992. Geoelectrical studies of the Colônia impact structure, São Paulo, state of São Paulo, Brazil. Rev. Bras. Geof. 10, 25–41.
Marvin, U.B., Einaudi, M.T., 1967. Black, magnetic spherules from Pleistocene and recent beach sediments. Geochem. Cosmochem. Acta 31, 1871–1884.
Melosh, H.J., 1989. Impact cratering: a geologic process. In: Research Supported by NASA, vol. 11. Oxford University Press (Oxford Monographs on Geology and Geophysics, New York.
Motta, U.S., Flexor, J.M., 1991. Estudo gravimétrico da depressão circular de Colônia, São Paulo, Brasil. Anais do 2º Congr. Inter. Soc. Bras. Geof., Salvador 140–142.
Murray, J., Renard, A.F., 1891. Chemical composition of manganese nodules and other manganese rich deposits discovered during the HMS Challenger expedition. PANGAEA. https://doi.org/10.1594/PANGAEA.849018.
Neves, F.A., 1998. Estudo da depressão circular de Colônia, SP, pelo método sísmico. Rev. Bras. Geoc. 28, 3–10.
Niyogi, A., Pat, J.K., Patel, S.C., Panda, D., Patil, S.K., 2011. Anthropogenic and impact spherules: morphological similarity and chemical distinction – a case from India and its implications. J. Earth Syst. Sci. 120, 1043–1054.
Osinski, G.R., Pierazzo, E. (Eds.), 2012. Impact Cratering: Processes and Products. John Wiley & Sons, Ltd., UK https://doi.org/10.1002/9781118447307.
Prasad, M.S., Khedekar, V.D., 2003. Impact microcrater morphology on Australasian microtektites. Meteorit. Planet. Sci. 38, 1351–1371.
Prasad, M.S., Sudhakar, M., 1998. Microimpact phenomena on Australasian microtektites: implications for ejecta plume characteristics and lunar surface processes. Meteorit. Planet. Sci. 33, 1271–1279.
Riccomini, C., Crósta, A.P., Prado, R.L., Ledru, M.P., Turcq, B.J., Sant'Anna, L.G., Ferrari, J.A., Reimold, W.U., 2011. The Colônia structure, São Paulo, Brazil. Meteorit. Planet. Sci. 46, 1630–1639.
Riccomini, C., Neves, F.A., Turcq, B.J., 1992. Astroblema de Colônia (São Paulo, Brasil). Estágio atual de conhecimento. 37º Congr. Bras. Geol. São Paulo. Roteiros de Excursões, p. 14.
Riccomini, C., Turcq, B.J., Ledru, M.P., Sant'Anna, L.G., Ferrari, J.A., 2005. Cratera de Colônia, SP. Provável astroblema com registros do paleoclima quaternário na Grande São Paulo. In: Winge, M., Schobbenhaus, C., Berbert-Born, M., Queiroz, E.T., Campos, D.A., Souza, C.R.G. (Eds.), Sítios Geol. Arqueol. Bras., Brasília, vol. 2. CPRM/SIGEP, pp. 35–44.
Riccomini, C., Turcq, B.J., Martin, L., 1989. The Colônia astrobleme. International Symposium on Global Changes in South America during the Quaternary: Past, Present and Future. ABEQUA/INQUA, Excursion Field Guide, São Paulo, p. 14.
Riccomini, C., Turcq, B.J., Moreira, M.Z., Lorscheitter, M.L., 1991. The Colônia astrobleme, Brazil. Rev. Inst. Geol. 12, 87–94.
Simonson, B.M., Glass, B.P., 2004. Spherule layers-records of ancient impacts. Annu. Rev. Earth Planet Sci. 32, 329–361.
Stauffer, M.R., Butler, S.L., 2010. The shapes of splash-form tektites: their geometrical analysis, classification and mechanics of formation. Earth Moon Planets 107, 169–196. https://doi.org/10.1007/s11038-010-9359-y.
Stöffler, D., Grieve, R.A.F., 2007. Impactites. In: Fettes, D., Desmons, J. (Eds.), Metamorphic Rocks, a Classification and Glossary of Terms. Cambridge University Press, Cambridge, pp. 82–92.
Velázquez, V.F., Barros, J.B., Riccomini, C., Hachiro, J., Sant'Anna, L.G., 2008. A cratera de Colônia: herança geológica e patrimônio natural na zona sul da região metropolitana de São Paulo. 44º Congr. Bras. Geol., Curitiba, CD-ROM.
Velázquez, V.F., Collona, J., Sallun, A.E.M., Azevedo Sobrinho, J.M., Sallun Filho, W., Paiva Jr., P.C.A., 2014. The Colônia impact crater: geological heritage and natural patrimony in the Southern metropolitan region of São Paulo, Brazil. Geoheritage 6, 283–290.
Velázquez, V.F., Hachiro, J., Riccomini, C., Sant'Anna, L.G., Godoy, S.A.P., 2006. A cratera de Colônia como parque temático e georrecurso. 43º Congr. Bras. Geol., Aracaju, CD-ROM.
Velázquez, V.F., Lucena, R.F., Azevedo Sobrinho, J.A., Martins Sallun, A.E., Sallun Filho, W., 2018. Petrographic investigation of target rock transformation under high shock pressures from the Colônia impact crater, Brazil. Earth Res. Sci. 7 (1), 13–24.
Velázquez, V.F., Riccomini, C., Azevedo Sobrinho, J.M., Rankin, A.S., Sallun, A.M.E., Hachiro, J., Sant'Anna, L.G., 2010. Microscopic Evidence of Shock Metamorphism Effects in Detrital Minerals from the Colônia Crater Sediments. 45º Congr. Bras. Geol., Belém, CD-ROM.
Velázquez, V.F., Riccomini, C., Azevedo Sobrinho, J.M., Pletsch, M.A.J.S., Sallun, A.E.M., Sallun Filho, W., Hachiro, J., 2013. Evidence of shock metamorphism effects in allocthonous breccia de deposits from the Colônia crater, São Paulo Brazil. Inter. J. Geosci. 4, 274–282.
Wagstaff, J., King, E.A., 1981. Micrometeorites and possible cometary dust from Antarctic ice cores. Lunar Planet. Sci. 12, 1124–1126.
Wu, Y., Sharmaa, M., LeCompteb, M.A., Demitroffc, M.N., Landis, J.D., 2013. Origin and provenance of spherules and magnetic grains at the Younger Dryas boundary. Proc. Natl. Acad. USA 110 (38), E3557–E3566. https://doi.org/10.1073/pnas.1304059110.
Xu, J.J., 2004. Dynamical Theory of Dendritic Growth in Convective Flow. Kluwer Academic Publishers, New York.
Zhang, H., Shen, S., Cao, C., Zheng, Q., 2014. Origins of microspherules from the Permian–Triassic boundary event layers in South China. Lithos 204, 246–257.